VETOR

Modeling and Simulation of Fluid Flow Dynamics for CO_2 Migration in Two-Dimensional Saline Aquifers☆

Modelagem e Simulação da Migração de CO_2 em Aquíferos Salinos

Henglai Zhai[1], Zaibin Lin[1], Francisco Oliveira[2], Jefferson Gomes[1,†]

[1]*Fluid Mechanics Research Group, School of Engineering, University of Aberdeen, UK*
[2]*State University of Santa Cruz, Brazil*
[†]**Corresponding author:** jefferson.gomes@abdn.ac.uk

Abstract

Geological carbon sequestration is increasingly recognized as a promising solution for mitigating CO_2 emissions by storing CO_2 in geological formations such as saline aquifers. Although recent research has primarily focused on optimizing CO_2 trapping mechanisms to enhance storage efficiency, flow dynamics of CO_2 plume migration – particularly the propagation and growth of fingers – remain insufficiently understood. In response to these challenges, we developed a model to simulate CO_2 plume migration in porous media within two-dimensional (2D) saline aquifers. This study utilizes high-order accurate reservoir simulations within the ICFERST framework – a control volume finite element method (CVFEM) formulation to specifically capture viscous instabilities associated with CO_2 plume migration. The simulation process integrates various mesh resolutions and incorporates adaptive mesh optimization (AMO). Our results indicate that increasing mesh resolution significantly enhances the ability to accurately capture the formation and growth of CO_2 fingers. In homogeneous porous media, AMO effectively balances accuracy and computational efficiency by dynamically refining or coarsening the mesh in critical regions. In heterogeneous porous media, simulations reveal the emergence of wider and larger fingers compared to those observed in homogeneous settings, with bifurcations occurring at locations where relative permeability undergoes significant changes.

Keywords

CO_2 sequestration • CO_2 Plume migration • Saffman-Taylor instability • Finger growth

Resumo

A captura geológica de carbono é cada vez mais reconhecida como uma solução promissora para mitigar as emissões de CO_2 através do armazenamento de CO_2 em formações geológicas, como aquíferos salinos. Embora pesquisas recentes tenham se concentrado principalmente na otimização dos mecanismos de captura de CO_2 para melhorar a eficiência de armazenamento, a dinâmica de fluxo da migração da pluma de CO_2, especialmente a propagação e o crescimento de interdigitações gasosas, ainda é pouco compreendida. Em resposta a esses desafios, um modelo numérico foi desenvolvido para simular a migração da pluma de CO_2 em meios porosos em aquíferos salinos bidimensionais (2D). Este estudo utiliza simulações de reservatório de alta ordem de precisão dentro da estrutura ICFERST – uma formulação do método de elementos finitos de volume de controle (CVFEM), para capturar instabilidades viscosas associadas à migração da pluma de CO_2. O processo de simulação integra várias resoluções de malha e incorpora otimização adaptativa de malha (AMO). Nossos resultados indicam que o aumento da resolução da malha melhora significativamente a capacidade de capturar com precisão a formação e o crescimento das interdigitações viscosas de CO_2. Em meios porosos homogêneos, o AMO equilibra a precisão e a eficiência computacional,

☆This article is an extended version of the work presented at the Joint XXVII ENMC National Meeting on Computational Modeling, XV ECTM Meeting on Science and Technology of Materials,held in Ilhéus–Brazil,from October 1st to 4th,2024.

refinando ou engrossando dinamicamente a malha em regiões críticas (*i.e.*, em regiões de interface) . Em meios porosos heterogêneos, as simulações revelam o surgimento de interdigitações viscosas mais largas e maiores em comparação com aqueles observados em configurações homogêneas, com bifurcações ocorrendo em locais onde a permeabilidade relativa sofre mudanças significativas.

Palavras-chave

Sequestro de CO_2 • Pluma de CO_2 • Instabilidade de Saffman-Taylor • Interdigitação viscosa

1 Introduction

The increase in atmospheric greenhouse gases, driven primarily by anthropogenic carbon dioxide (CO_2) emissions, is a well-known contributor to global warming. To mitigate these emissions and achieve net-zero carbon targets, geological carbon sequestration has emerged as a promising technology. Among the various options for CO_2 storage, deep saline aquifers are particularly attractive due to their substantial global storage capacity. These aquifers are typically capped by impermeable sedimentary layers known as caprock, and they often exhibit conditions that favor the storage of CO_2 in its supercritical phase [1]. Upon injection into deep saline aquifers, CO_2 migrates radially from high-pressure injection points to regions of lower pressure, as illustrated in Fig. 1, following Darcy's Law. During this advection process, Saffman-Taylor instabilities, characterized by the formation and growth of finger-like patterns at the fluid interface, can occur. These instabilities are critical as they influence the migration and potential trapping of the CO_2 plume within the geological formation. The Saffman-Taylor instability (STI), also known as

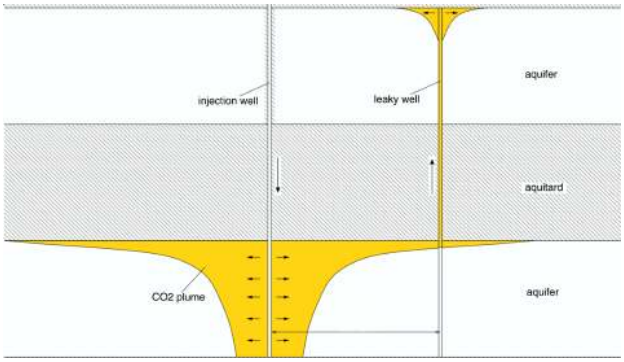

Figure 1: Migration of CO_2 plume at the reservoir with injection and leaky well [2].

viscous fingering instability, describes the pattern formation that arises at an unstable interface between two fluids flowing in porous media. Firstly mathematically characterized by Saffman and Taylor [3], STI occurs when a less viscous fluid is injected to displace a more viscous one. Over time, the less viscous fluid penetrates the more viscous fluid, resulting in the development of finger-like patterns.

Recent studies have explored various aspects of STI. For example, Langtangen et al. [4] investigated fluid flow dynamics in heterogeneous porous media, revealing the inherent instability of the hyperbolic Buckley-Leverett model, where even slight perturbations in physical properties could disrupt the expected uniform interface. Analytical and semi-analytical solutions by Nordbotten et al. [5] and Vilarrasa et al. [6] predicted the location of the interface between the brine formation and CO_2 rich phases, accounting for the viscosity and density contrasts. Hidalgo et al. [7] used numerical simulations to examine CO_2 dissolution flux in homogeneous media, while Pramanik and Mishra [8] studied vertical flow instabilities under varying flow velocities in fluids with different densities and viscosities. Norouzi and Shoghi [9] examined the impact of fluid elasticity on miscible displacement within a Hele-Shaw cell, using Boger fluids as displaced medium and comparing the results with Newtonian fluids. Similarly, Yazdi and Norouzi [10] provided a numerical analysis of STI in immiscible viscoelastic-Newtonian displacement within a Hele-Shaw cell, employing the Giesekus model to describe nonlinear viscoelastic behavior and using a parallelized finite volume method (FVM) for simulation. Their results indicated that both fluid elasticity and capillary number could mitigate the severity of STI. More recently, Bonazzi et al. [11] analyzed the transport from an initial ellipse-shaped solute source, exploring the impact of varying the mean flow velocity in both homogeneous and heterogeneous porous media. Furthermore, Pouplard and Tsai [12] demonstrated experimentally and theoretically that fingering instabilities in complex fluids could be suppressed or controlled using a radially tapered cell, achieving stable interfaces at low flow rates and steeper gradients.

Despite significant progress in understanding the factors influencing STI, the physics governing the growth and propagation of fingers during unstable displacements remains incompletely understood. Furthermore, many studies

on CO_2 migration have focused on idealized formations, with a predominant emphasis on homogeneous porous media. The impact of the medium's heterogeneity, despite its importance, continues to present significant challenges. Furthermore, in numerical simulations of geofluid dynamics, the variability of fluid properties is often overlooked due to the use of coarse computational mesh grids [13].

In response to these challenges, we develop a comprehensive model to simulate CO_2 plume migration within both homogeneous and heterogeneous porous media in two-dimensional (2D) saline aquifers that contain a leaky well. This work focuses on employing high-order accurate reservoir simulations using the ICFERST [14] framework, specifically targeting the modeling of viscous instabilities that arise during CO_2 plume migration. To enhance the balance between accuracy and computational efficiency, we incorporate adaptive mesh optimization throughout the simulation process.

The structure of this paper is organized as follows: Section 2 provides a detailed summary of the computational model and numerical methods utilized in this study. Section 3 outlines the numerical experiments setup, including the properties of the fluids and the parameters that characterize the 2D saline aquifers. The results of our simulations are presented and discussed in Section 4, followed by the conclusions in Section 5.

2 Multi-Fluid Flow Model

2.1 Force Balance and Transport Model

The flow of immiscible fluids in two phases through a porous medium domain Ω (where $\boldsymbol{x} \in \Omega$ and $t > 0$) can be described by the extended Darcy's law and saturation equations [13],

$$\mu_\alpha S_\alpha \left(\boldsymbol{K}\mathcal{K}_{r,\alpha}\right)^{-1} \boldsymbol{u}_\alpha = \underline{\underline{\sigma}}_\alpha \boldsymbol{u}_\alpha = -\nabla p + \boldsymbol{S}_{u,\alpha}, \tag{1}$$

$$\phi \frac{\partial S_\alpha}{\partial t} + \nabla \cdot (\boldsymbol{u}_\alpha S_\alpha) = \mathcal{S}_{cty,\alpha}. \tag{2}$$

In these equations, μ_α denotes the viscosity, $\boldsymbol{K}$ represents the absolute permeability, p is the pressure, and ϕ is the porosity, $\mathcal{K}_{r,\alpha}$ represents the α-phase relative permeability. Additionally, S_α denotes saturation, subject to the mass conservation constraint $\sum_{\alpha=1}^{\mathcal{N}_i} S_\alpha = 1$ (where $\mathcal{N}_i$ denotes the number of phases). Finally, the term $\boldsymbol{u}_\alpha$ indicates the saturation-weighted Darcy velocity, $\underline{\underline{\sigma}}_\alpha$ is an absorption-like term that accounts for the implicit linearization of the viscous frictional forces. Source terms, $\boldsymbol{S}_{u,\alpha}$ and $\mathcal{S}_{cty,\alpha}$, correspond to the α-phase contributions in the momentum (e.g., gravity, capillary forces, etc.) and continuity (e.g., mass transfer across fluids/phases, geochemical reactions, etc.) equations, respectively.

2.2 Discretization and Numerical Formulation

By testing with the velocity basis-function space, the following integral equation for each element E is obtained:

$$\sum_E \int_{\Omega_E} Q_i \left(\boldsymbol{v}_\alpha + \nabla p - \boldsymbol{S}_{u,\alpha}\right) dV + \oint_{\Gamma_E} Q_i \boldsymbol{n} (p - \tilde{p})\, d\Gamma + \oint_{\Gamma_\Omega} Q_i \boldsymbol{n} (p - p_{\text{bc}})\, d\Gamma = \boldsymbol{0} \tag{3}$$

where, Ω_E and Γ_E denote the volume and boundary of element E, respectively; Γ_Ω represents the model boundary of the computational domain. The numerical pressure $\tilde{p}$ appearing in the jump condition is the arithmetic mean of the potentially discontinuous pressure across the element E; p_{bc} is the specified pressure boundary conditions and $\boldsymbol{n}$ is the normal to the element boundary. This equation can be expressed in matrix form at the time level $n+1$ as:

$$\boldsymbol{M}\underline{\boldsymbol{v}} = -\boldsymbol{C}\underline{\boldsymbol{p}} + \underline{\boldsymbol{s}}_u. \tag{4}$$

Similarly, Eq. 2 is discretized in space by testing the weak form of the equation over each control volume (CV) using CV-basis functions M_i. Summing over all phases and discretizing in time using the θ-method yields the global mass-balance equation:

$$\sum_{\alpha=1}^{\mathcal{N}_\alpha} \int_\Omega M_i \frac{\phi \left(S_{\alpha i}^{n+1} - S_{\alpha i}^{n}\right)}{\Delta t} dV + \oint_{\Gamma_{CV_i}} \left[\theta^{n+\frac{1}{2}} \boldsymbol{n} \cdot \boldsymbol{u}_\alpha^{n+1} S_\alpha^{n+1} + \left(1 - \theta^{n+\frac{1}{2}}\right) \boldsymbol{n} \cdot \boldsymbol{u}_\alpha^{n} S_\alpha^{n}\right] d\Gamma - \int_\Omega M_i \mathcal{S}_{cty,\alpha}^{n+\theta} dV = 0 \tag{5}$$

where, Ω_{CV_i} and Γ_{CV_i} are the volume and boundary of control volume i, respectively, and $\boldsymbol{n}$ is the normal vector to the CV boundary. The weighting parameter θ varies smoothly between 0.5, corresponding to the Crank–Nicolson

method, and 1, corresponding to the backward-Euler scheme, to mitigate the introduction of spurious oscillations at large grid Courant numbers. This equation can be expressed in matrix form at the time level $n+1$ as:

$$\boldsymbol{B}^{\mathrm{T}}\underline{\boldsymbol{v}}^{n+1} = \underline{\boldsymbol{s}}_p. \tag{6}$$

The pressure is obtained by combining Eqs. 4 and 6 to eliminate the velocity, yielding:

$$\boldsymbol{B}^{\mathrm{T}}\boldsymbol{M}^{-1}\boldsymbol{C}\,\underline{\boldsymbol{p}}^{n+1} = \underline{\boldsymbol{s}}_p^{n+1} - \boldsymbol{B}^{\mathrm{T}}\boldsymbol{M}^{-1}\underline{\boldsymbol{s}}_{\boldsymbol{u}}^{n+1}. \tag{7}$$

This equation can be solved using a multigrid-type approach to get the pressure and velocity.

The control volume finite element method (CVFEM) integrates FEM and FVM, and the primary advantage of it is that it produces a mass-conservative velocity field while maintaining the flexibility inherent in the finite element approach. Typically, pressure and velocity, and material properties, such as permeability and porosity, are represented FE-wise, but mass conservative properties such as saturation and concentration are represented CV-wise.

Cotter *et al.* [15] developed a family of $P_N(DG)-P_{N+1}$ triangle element types (some examples can be seen in Fig. 2). The velocity is represented by a discontinuous Nth-order polynomial, while pressure is continuous polynomial with an order of $N+1$. Mass balance equations are solved in control volume (CV) space using a discontinued Petrov-Galerkin FEM formulation to obtain high-order accurate velocities on CV boundaries, ensuring bounded solutions. The number of pressure nodes per element (tetrahedral for 3D or triangle for 2D) depends on the order $Z(=N+1)$ of the basis functions.

For higher-order accurate elements, additional pressure and velocity nodes are on the edges. For example, the pair of elements $P_1(DG)-P_2$ $(N=1)$ has a linear-discontinuous basis function for velocity $P_1(DG)$ and a quadratic-polynomial basis function for pressure (P_2), with pressure nodes at the corners and midpoints of the edges, and velocity nodes at corners. Results are obtained using mesh elements of varying order, from $N=0$ to $N=2$. CVs are formed around pressure nodes, so the number of CVs per element also depends on the order Z.

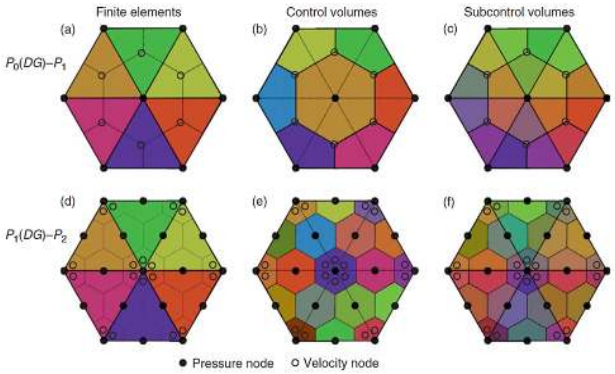

Figure 2: Examples of 2D elements: (a-c) show $P_0(DG)-P_1$, (d-f) show $P_1(DG)-P_2$ elements. [16]

Therefore, this method is highly effective at preventing numerical diffusion without the need for mesh refinement at discontinuities. However, a significant drawback of this approach is its computational expense, which arises from global duplication of pressure and velocity nodes, as well as the necessity for higher-order accurate velocity approximations to ensure stability.

The CVFEM-based ICFERST model is an open-source code (licensed under the Lesser General Public License, LGPL). It employs a metric tensor field based on solution interpolation error estimates to manage local mesh topology effectively [16]. Unlike conventional flow simulators, which confine the geological domain within predefined surfaces and represent faults with additional surfaces, ICFERST leverages adaptive mesh optimization (AMO) to enhance computational quality. This technique generates finer unstructured meshes in regions with rapid flow property variations and coarser meshes in areas with more gradual changes [17]. By dynamically adapting the mesh in both space and time, the model provides targeted resolution where it is most needed, such as near concentration or saturation fronts. The use of fully unstructured tetrahedral/triangular finite elements further enhances geometric flexibility, enabling accurate representation of complex geological structures and internal boundaries. This advanced meshing strategy significantly improves the precision and efficiency of flow simulations in reservoirs.

Table 1: Summary of parameters used in numerical simulations. Superscript o denotes initial condition, K_i is in m^2 and u_w^o is in m/s. $\mathcal{K}^\circ_{r,nw}$, $\mathcal{K}^\circ_{r,w}$,$S_{w,irr}$, $S_{nw,r}$ are the same for all simulations (Eq. 8). VR is viscosity ratio.

ϕ	VR	S_w^o	S_{nw}^o	$S_{w,irr}$	$S_{nw,r}$	K_1	K_2	K_3	K_4	K_5	u_w^o
0.2	≈ 10	0	1.0	0.2	0.2	10^{-15}	10^{-14}	10^{-13}	10^{-12}	10^{-11}	5.4×10^{-3}

Table 2: Properties of CO_2 and Brine

T(K)	Initial P(MPa)	CO_2 Density(kg m^{-3})	CO_2 Viscosity(Pa·s)	Water/Brine Density (kg m^{-3})	Water/Brine Viscosity (Pa·s)
400	10	161.53	2.25×10^{-5}	937.87 / 1027.61	2.19×10^{-4} / 2.50×10^{-4}

3 Description of the Numerical Experiments

3.1 Densities and Viscosities of CO_2 and Brine

The accuracy of these properties significantly influences CO_2 plume flow behavior and flow instabilities. The most precise equations of state (EoS) for pure CO_2 and water across a wide range of pressure-temperature (P-T) conditions are the Span-Wagner EoS and the IAPWS-95 EoS, respectively. Calculations of densities and viscosities for both water and CO_2 can be facilitated using the C++ library CoolProp [18, 19]. For pure CO_2, CoolProp utilizes the Span-Wagner EoS [20] and the viscosity model proposed by Laesecke and Muzny [21].

For pure water, the EoS is based on the formulation by Wagner and Pruß [22], which adheres to the thermodynamic formulation for water properties from the International Association for the Properties of Water (IAPWS-95), and the viscosity model by Huber *et al.* [23]. To determine the density of brine, the correlation proposed by Andersen *et al.* [24] is employed. For the viscosity of brine, the model developed by Mao and Duan [25] is used and this model is applicable to ionic strengths of slutions with concentration of up to 6 molal.

In this work, several assumptions are made for brine displacement by CO_2 flows:

- Brine is considered incompressible, with both constant density and viscosity;
- CO_2 is treated as a compressible fluid: the Random Forest (RF) algorithm is employed to train the density model over a wide range of *P-T* conditions, mitigating the abrupt changes associated with phase change; the viscosity of CO_2 is assumed constant as it exhibits minimal variation with pressure;
- CO_2 and brine are assumed to form an ideal mixture, with no chemical or physical interactions between them;
- CO_2 displacement of brine is considered an isothermal process.

3.2 Relative Permeability Model

Relative permeability $\mathcal{K}_r$ quantifies the ability of one fluid to flow relative to another fluid within a porous medium. It is defined as $\mathcal{K}_r = \mathcal{K}_{\text{eff}}/\mathcal{K}_{\text{abs}}$, where $\mathcal{K}_{\text{eff}}$ is the effective permeability of the fluid, and $\mathcal{K}_{\text{abs}}$ is the absolute permeability (K) of the medium. In this paper, the modified Corey-Brooks model [26] was used,

$$\begin{aligned} \mathcal{K}_{rw}(S_w) &= \mathcal{K}^\circ_{rw}\left[\frac{S_w - S_{w,\text{irr}}}{1 - S_{w,\text{irr}} - S_{nw,r}}\right]^{n_w}, \\ \mathcal{K}_{rnw}(S_{nw}) &= \mathcal{K}^\circ_{rnw}\left[\frac{S_{nw} - S_{nw,r}}{1 - S_{w,\text{irr}} - S_{nw,r}}\right]^{n_{nw}}. \end{aligned} \tag{8}$$

where subscripts w and nw denote the wetting and non-wetting phases, respectively. $\mathcal{K}^\circ_{r,w}$ and $\mathcal{K}^\circ_{r,nw}$ represent the relative permeability of the end point for the wetting and non-wetting phases. $S_{w,\text{irr}}$ and $S_{nw,r}$ refer to the irreducible wetting phase saturation and the residual non-wetting phase saturation, respectively. The exponents n_w and n_{nw} are both set to 2, and the end-point relative permeabilities $\mathcal{K}^\circ_{r,w}$ and $\mathcal{K}^\circ_{r,nw}$ are both set to 1. Other parameters are detailed in Table 1.

3.3 Model Set-up

In this work, 2D simulations are conducted in a horizontal square region (5×5 m with an injection well and a leakage well) of a deep saline aquifer, where the pressure is about 10 MPa and the temperature is approximately 400 K. For all simulations, the domain was initially saturated with 1 mol kg^{-1} NaCl brine. This non-wetting fluid was subsequently displaced by a pure supercritical CO_2 at a specified initial velocity u_w^o. For simplicity, the effects of gravity and capillary pressure were neglected. The initial setup, including porosity, absolute permeability for the numerical simulations, is summarized in Table 1 while properties of CO_2 and brine are summarized in Table 2. The absolute permeability (K) was considered constant in some simulations, while in others, it was spatially variable, represented as $\boldsymbol{K} = \boldsymbol{K}(x_i)$.

All test cases were conducted within an idealized geological formation, discretized using unstructured triangular meshes. The $P_1(DG)-P_2$ finite element pairs, as illustrated in Fig. 2d-f, were used to discretize and solve Equations 1 and 2. Additionally, simulations employed an adaptive time-stepping based on a modified Crank-Nicolson θ method with a minimum time step of 0.1, incorporating an a posteriori adaptive time step size to adhere to the Courant-Friedrichs-Lewy (CFL) condition (≤ 1).

4 Results

4.1 Fingering Growth at Fixed and Adaptive Mesh

Mesh resolution is critical in the simulation of grid models, especially in studies that focus on the development of fingers in immiscible displacement. Higher mesh resolution improves the accuracy to capture formation and growth of these fingers.

In this section, numerical simulations with viscosity ratio (VR = 10) were conducted using fixed and adaptive mesh resolutions to qualitatively assess the ability of the model to capture finger formation. Figure 3 illustrates numerical simulations performed with varying mesh resolutions, ranging from significantly lower to higher resolutions (i.e., from 3351 to 82136 elements). As evidenced, lower mesh resolutions hinder the accurate capture of finger formation, growth, and branching. Conversely, higher mesh resolutions lead to a greater number of sharp and well-defined fingers. So, to accurately represent the continuous development of viscous instabilities, it is imperative to use mesh grids with adequate resolution at the fluid interfaces.

Moreover, an additional simulation was conducted with the same parameters as the previous simulations, but with an adaptive mesh resolution at the displacement front. In this simulation, the mesh grid adapts to oscillations in CO_2 phase saturation, characterized by the following parameters: (a) minimum element length of 0.005 unit-length and maximum element length of 0.1 unit-length, (b) maximum of 100k elements, and (c) prescribed interpolation error estimate of 5×10^{-3}. The results, depicted in Fig. 4, demonstrate a more pronounced formation and growth of fingers in the same region compared to Fig. 3. Additionally, the fingers are more sharply defined at the same observed time. This improvement is attributed to adaptive mesh optimization (AMO), which refines the mesh at the displacement front and coarsens it in other regions.

4.2 Fingering Growth at Heterogeneous Porous Media

Geological formations always show spatial variation on all length-scales characterized by small-scale heterogeneity. Fluid flow dynamics through heterogeneous porous media is significantly more complex than those through homogeneous media. The heterogeneity in the permeability parameter is a primary driver of fluid instability, as it creates preferential flow pathways that foster the formation and rapid growth of fingers.

To qualitatively assess the influence of heterogeneity, characterized by variations in permeability, a numerical simulation with VR=10 was conducted using specified permeability distributions. The absolute permeability was established with a Gaussian distribution with values ranging from 10^{-15} to 10^{-11} m^2 as shown in Fig. 5a. The simulations employed identical mesh resolution, boundary conditions, geometry, and initial conditions.

Figure 5 illustrates the development of multi-scale elongations, characterized by the continuous growth and merging of dendritic finger branches throughout the simulations. Simulations were performed in fixed mesh of 52k triangular $P_1(DG) - P_2$ element-pairs, with 2 permeability distributions (ranges of K_i are described in Table 1).

In these simulations, the maximum finger width reached approximately 1/4 of the entire area by 180 seconds, which is larger than those observed in other simulations. Furthermore, larger elongations are evident in the upper right region, and fingers bifurcate in regions of large permeability changes (center of the 2D formation). Permeability magnitude only affects the flow rate, while the extent of permeability variation influences finger's shape and size. And in geological formations, CO_2's tendency to traverse high-permeability zones can significantly influence its migration pathways and potential storage locations. As a result, the finger-like structures formed in heterogeneous media are significantly different from those observed in homogeneous media.

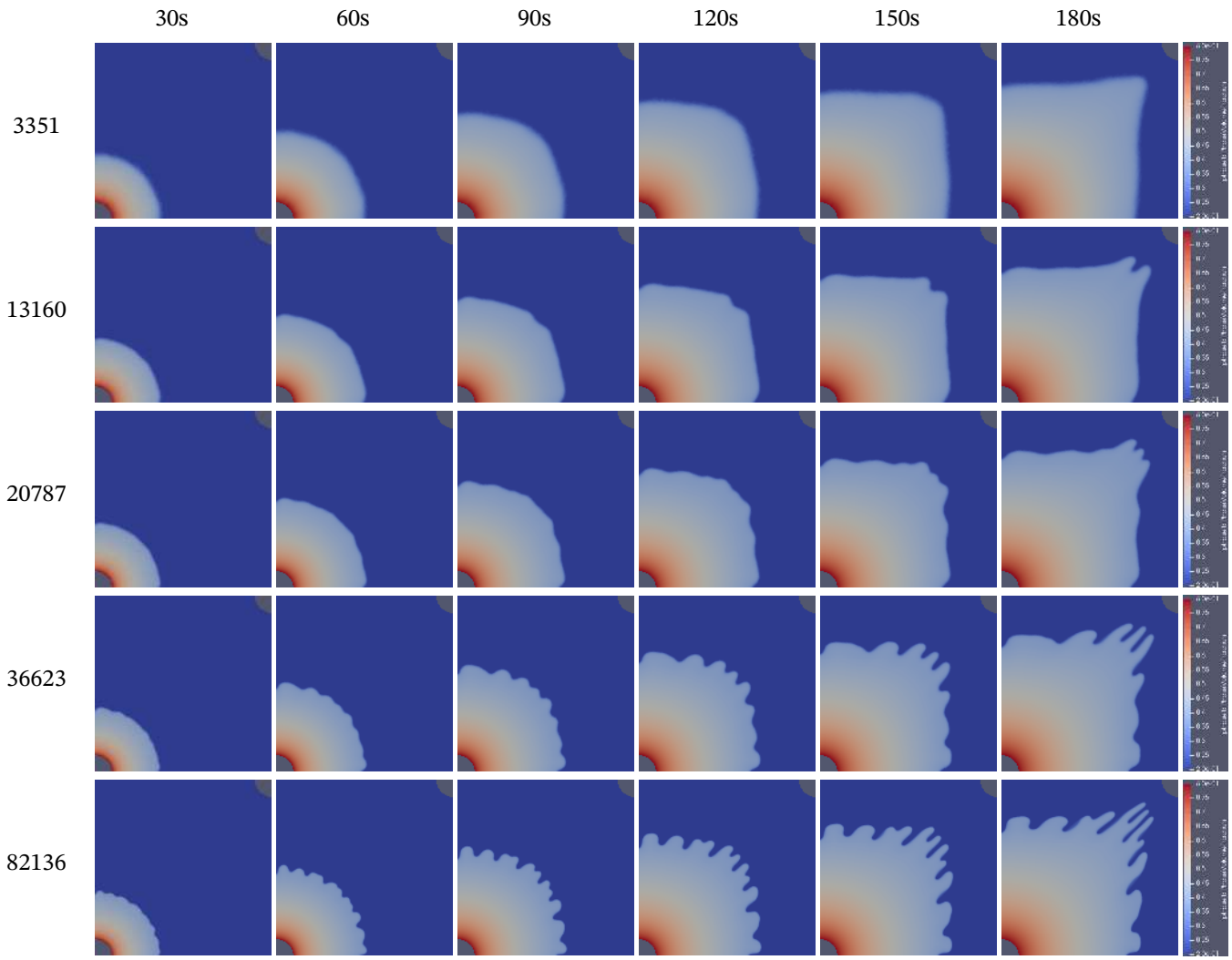

Figure 3: Simulated flow with VR=10 and K= 10^{-14} m^2 (homogeneous porous media): snapshots of saturation fronts at different time (top). The domain was discretized with several fixed mesh resolutions (from 3351 to 82136 elements) with $P_1(DG) - P_2$ element-pairs.

5 Conclusions

Technologies for CO_2 sequestration in deep saline aquifers through geological processes are essential components of carbon capture and storage (CCS) strategies, playing a critical role in reducing carbon emissions and combating global warming to achieve net-zero emissions. When CO_2 is injected into reservoirs, flow instabilities (Saffman-Taylor) emerge at the fluid interface during displacement in porous media. These instabilities, induced mainly by variations in viscosity, density and heterogeneity, result in the formation and growth of fingers.

This paper presents simulations analyzing the formation and growth of viscous fingers. These simulations investigate the effects of mesh resolutions in both ideal homogeneous and heterogeneous square formations, incorporating an injection well and a leakage well.

The results indicate that increasing mesh resolution enhances the accuracy in capturing the formation and growth of the CO_2 fingers. In simulations involving homogeneous porous media, adaptive mesh techniques effectively balance accuracy and computational efficiency by dynamically refining or coarsening the mesh in targeted regions. In heterogeneous porous media, the simulations reveal wider and larger fingers compared to those in homogeneous settings, with bifurcation occurring at locations where relative permeability changes significantly. This behavior is attributed to CO_2's tendency to migrate through high-permeability zones, which strongly influences its migration pathways and potential storage locations.

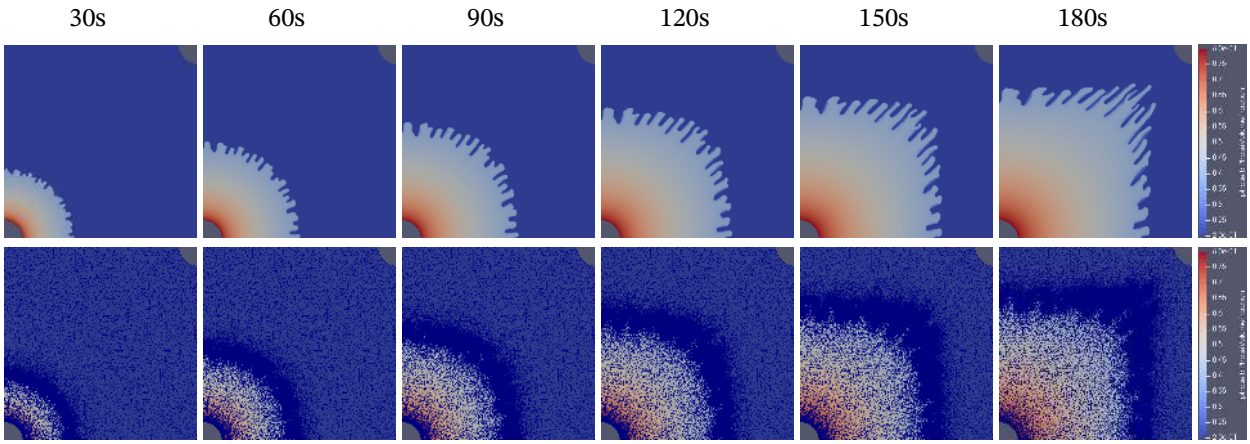

Figure 4: Simulated flow with VR=10 and K= 10^{-14} m^2 (homogeneous porous media): snapshots of saturation fronts at different time (top). The domain was discretized with adaptive mesh (with resolution ranging from 13k to 100k elements) with $P_1(DG) - P_2$ element-pairs. The bottom row shows saturation profile overlapped with mesh resolution.

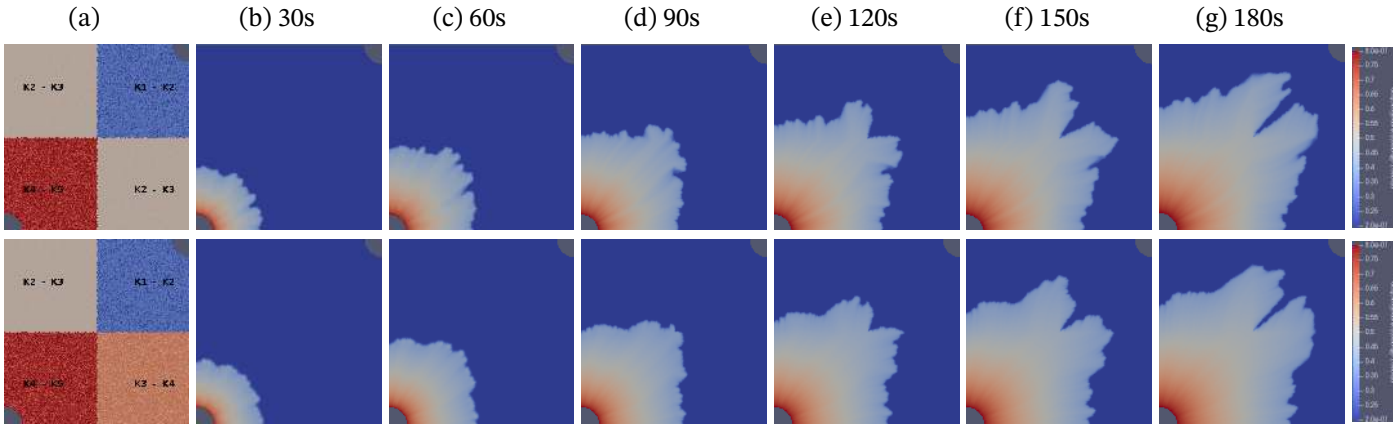

Figure 5: Simulated flow with VR=10 with (a) case scenarios of two permeability distributions (both heterogeneous porous media); (b-f) snapshots of saturation fronts at different time stamps. The domain was discretized with 52462 $P_1(DG) - P_2$ element-pairs (fixed mesh). Values of K_i are listed in Table 1.

Acknowledgements

The authors sincerely thank Stephen Aroh Ajah for his invaluable support and guidance on this research related to the random forest algorithm. We also appreciate the University of Aberdeen for providing essential resources and facilities. This work was financially supported by the China Scholarship Council, for which we are grateful.

References

[1] A. Peter, D. Yang, K. I.-I. I. Eshiet, and Y. Sheng, "A review of the studies on CO_2–brine–rock interaction in geological storage process," *Geosciences*, vol. 12, no. 4, p. 168, 2022. Available at: https://doi.org/10.3390/geosciences12040168

[2] H. Class, A. Ebigbo, R. Helmig, H. K. Dahle, J. M. Nordbotten, M. A. Celia, P. Audigane, M. Darcis, J. Ennis-King, Y. Fan *et al.*, "A benchmark study on problems related to CO_2 storage in geologic formations: summary and discussion of the results," *Computational geosciences*, vol. 13, pp. 409–434, 2009. Available at: https://doi.org/10.1007/s10596-009-9146-x

[3] P. G. Saffman and G. I. Taylor, "The penetration of a fluid into a porous medium or hele-shaw cell containing a more viscous liquid," *Proceedings of the Royal Society of London. Series A. Mathematical and Physical Sciences*, vol. 245, no. 1242, pp. 312–329, 1958. Available at: https://doi.org/10.1098/rspa.1958.0085

[4] H. P. Langtangen, A. Tveito, and R. Winther, "Instability of Buckley-Leverett flow in a heterogeneous medium," *Transport in Porous Media*, vol. 9, no. 3, pp. 165–185, 1992. Available at: https://doi.org/10.1007/BF00611965

[5] J. M. Nordbotten, M. A. Celia, and S. Bachu, "Injection and storage of CO_2 in deep saline aquifers: analytical solution for CO_2 plume evolution during injection," *Transport in Porous media*, vol. 58, pp. 339–360, 2005. Available at: https://doi.org/10.1007/s11242-004-0670-9

[6] V. Vilarrasa, D. Bolster, M. Dentz, S. Olivella, and J. Carrera, "Effects of CO_2 compressibility on CO_2 storage in deep saline aquifers," *Transport in porous media*, vol. 85, pp. 619–639, 2010. Available at: https://doi.org/10.1007/s11242-010-9582-z

[7] J. J. Hidalgo, C. W. MacMinn, and R. Juanes, "Dynamics of convective dissolution from a migrating current of carbon dioxide," *Advances in water resources*, vol. 62, pp. 511–519, 2013. Available at: https://doi.org/10.1016/j.advwatres.2013.06.013

[8] S. Pramanik and M. Mishra, "Coupled effect of viscosity and density gradients on fingering instabilities of a miscible slice in porous media," *Physics of Fluids*, vol. 28, no. 8, 2016. Available at: https://doi.org/10.1063/1.4961042

[9] M. Norouzi and M. R. Shoghi, "A numerical study on miscible viscous fingering instability in anisotropic porous media," *Physics of Fluids*, vol. 26, no. 8, 2014. Available at: https://doi.org/10.1063/1.4891228

[10] A. A. Yazdi and M. Norouzi, "Numerical study of Saffman–Taylor instability in immiscible nonlinear viscoelastic flows," *Rheologica Acta*, vol. 57, pp. 575–589, 2018. Available at: https://doi.org/10.1007/s00397-018-1101-0

[11] A. Bonazzi, B. Jha, and F. P. de Barros, "Influence of initial plume shape on miscible porous media flows under density and viscosity contrasts," *Journal of Fluid Mechanics*, vol. 972, p. A19, 2023. Available at: https://doi.org/10.1017/jfm.2023.710

[12] A. Pouplard and P. A. Tsai, "Controlling viscous fingering instabilities of complex fluids," *Scientific Reports*, vol. 14, no. 1, p. 2338, 2024. Available at: https://doi.org/10.1038/s41598-024-52218-w

[13] K. Christou, W. Radünz, B. Lashore, F. de Oliveira, and J. Gomes, "Numerical investigation of viscous flow instabilities in multiphase heterogeneous porous media," *Advances in Water Resources*, vol. 130, pp. 46–65, 2019. Available at: https://doi.org/10.1016/j.advwatres.2018.10.010

[14] NORMS/AMCG. (2024) ICFERST: Imperial College Finite Element Reservoir Simulator. Available at: http://multifluids.github.io/

[15] C. J. Cotter, D. A. Ham, C. C. Pain, and S. Reich, "LBB stability of a mixed galerkin finite element pair for fluid flow simulations," *Journal of Computational Physics*, vol. 228, no. 2, pp. 336–348, 2009. Available at: https://doi.org/10.1016/j.jcp.2008.09.014

[16] M. D. Jackson, J. R. Percival, P. Mostaghimi, B. S. Tollit, D. Pavlidis, C. C. Pain, J. L. Gomes, A. H. El-Sheikh, P. Salinas, A. H. Muggeridge *et al.*, "Reservoir modeling for flow simulation by use of surfaces, adaptive unstructured meshes, and an overlapping-control-volume finite-element method," *SPE Reservoir Evaluation & Engineering*, vol. 18, no. 02, pp. 115–132, 2015. Available at: https://doi.org/10.2118/163633-PA

[17] S. Geiger, S. Roberts, S. K. Matthäi, C. Zoppou, and A. Burri, "Combining finite element and finite volume methods for efficient multiphase flow simulations in highly heterogeneous and structurally complex geologic media," *Geofluids*, vol. 4, no. 4, pp. 284–299, 2004. Available at: https://doi.org/10.1111/j.1468-8123.2004.00093.x

[18] CoolProp. (2024) CoolProp. Available at: http://www.coolprop.org/

[19] I. H. Bell, J. Wronski, S. Quoilin, and V. Lemort, "Pure and pseudo-pure fluid thermophysical property evaluation and the open-source thermophysical property library coolprop," *Industrial & Engineering Chemistry Research*, vol. 53, no. 6, pp. 2498–2508, 2014. Available at: http://pubs.acs.org/doi/abs/10.1021/ie4033999

[20] R. Span and W. Wagner, "A new equation of state for carbon dioxide covering the fluid region from the triple-point temperature to 1100 K at pressures up to 800 MPa," *Journal of physical and chemical reference data*, vol. 25, no. 6, pp. 1509–1596, 1996. Available at: https://doi.org/10.1063/1.555991

[21] A. Laesecke and C. D. Muzny, "Reference correlation for the viscosity of carbon dioxide," *Journal of physical and chemical reference data*, vol. 46, no. 1, 2017. Available at: https://doi.org/10.1063/1.4977429

[22] W. Wagner and A. Pruß, "The IAPWS formulation 1995 for the thermodynamic properties of ordinary water substance for general and scientific use," *Journal of physical and chemical reference data*, vol. 31, no. 2, pp. 387–535, 2002. Available at: https://doi.org/10.1063/1.1461829

[23] M. L. Huber, R. A. Perkins, A. Laesecke, D. G. Friend, J. V. Sengers, M. J. Assael, I. N. Metaxa, E. Vogel, R. Mareš, and K. Miyagawa, "New international formulation for the viscosity of H_2O," *Journal of Physical and Chemical Reference Data*, vol. 38, no. 2, pp. 101–125, 2009. Available at: https://doi.org/10.1063/1.3088050

[24] G. Andersen, A. Probst, L. Murray, and S. Butler, "An accurate PVT model for geothermal fluids as represented by H_2O-CO_2-NaCl mixtures," in *University of North Texas Libraries, UNT Digital Library*. UNT Libraries Government Documents Department, 1992. Available at: https://digital.library.unt.edu/ark:/67531/metadc885359/m1/1/

[25] S. Mao and Z. Duan, "The viscosity of aqueous alkali-chloride solutions up to 623 K, 1,000 bar, and high ionic strength," *International Journal of Thermophysics*, vol. 30, pp. 1510–1523, 2009. Available at: https://doi.org/10.1007/s10765-009-0646-7

[26] R. H. Brooks and A. T. Corey, *Hydraulic Properties of Porous Media*, ser. Hydrology Papers ; no. 3. Fort Collins, CO: Colorado State University, Hydrology and Water Resources Program, 1964. Available at: https://www.proquest.com/books/hydraulic-properties-porous-media-r-h-brooks-t/docview/47928924/se-2?accountid=8155